Available online at www.sciencedirect.com
SCIENCE DIRECT®

Journal of the European Ceramic Society 24 (2004) 119–127

www.elsevier.com/locate/jeurceramsoc

$CaZrO_3$, a Ni-co-sinterable dielectric material for base metal-multilayer ceramic capacitor applications

M. Pollet*, S. Marinel, G. Desgardin

CRISMAT Laboratory, UMR 6508 CNRS/ISMRA, 6 B^d du M^al Juin, 14050 Caen, France

Received 20 October 2002; received in revised form 18 February 2003; accepted 22 February 2003

Abstract

The aim of this work is to obtain $CaZrO_3$ powders that are co-sinterable with nickel electrodes. Since $CaZrO_3$ is often sintered at temperatures higher than 1550 °C to achieve high sample densities, obtaining a powder co-sinterable with Ni would require lower sintering temperatures. The co-sintering also requires that the reaction takes place in a reducing atmosphere. After optimizing the thermal cycle for the phase synthesis, several approaches were investigated to decrease the $CaZrO_3$ sintering temperature. First, the grain size effect on the densification was studied to enhance the calcined powder's reactivity before sintering. In addition, the Ca/Zr ratio was investigated, and the effect of doping with lithium salts was examined. Similarly, in order to allow co-sintering with base-metal inner electrodes, the sinterability and the properties of the dielectric were examined in a reducing atmosphere. Finally, a co-sintered material was synthesized, resulting in good dielectric properties. The samples were analyzed in terms of structure and microstructure. The electric and dielectric properties were also measured on sintered samples.

Keywords: BME-MLCC; $CaZrO_3$; Co-sintering; Nickel electrode; Reducing atmosphere

1. Introduction

For the past 3 years, the multilayer ceramic capacitor (MLCC) market has been growing in pace with the exponential development of the communications. The production of MLCCs has witnessed an annual growth near 150%. However, almost half of this production is based on noble metals (Pt, Pd, Ag), which are expensive. The market is open for the development of cheaper base metal electrodes MLCCs (BME-MLCCs). These new components essentially consist of nickel internal electrodes and are mostly implanted in type II MLCCs market.

The aim of this work is to discuss the feasibility of a type I BME-MLCC (higher temperature and frequency stability) with a high dielectric permittivity, manufactured with Ni electrodes and usable in the high frequency range. The dielectric material chosen for this study is the $CaZrO_3$ perovskite material. Calcium zirconate, $CaZrO_3$, is an interesting material for both mechanical (filters,[1] coatings[2]) and electrical applications (resonators, capacitors[3–5]). This material has recently been studied for its high performance as an ionic conductor for the solid electrodes in fuel cells.[6–9] In the case of passive components, it displays a high permittivity (around 30), low losses and a good behavior under electrical field and versus temperature. These properties allow its use in NPO-type multilayer ceramic capacitors (Negative–Positive–Zero).

The manufacturing of BME-MLCCs presents essentially two problems: first, the base metals used in the cofiring process (generally Ni, eventually Cu) are very sensitive to oxidation and the final component must therefore be fired in a reducing atmosphere. Second, these metals have low melting points (1453 °C for Ni and 1083 °C for Cu) which requires a decrease in the sintering temperature of the dielectric. The first point has been extensively studied, especially in the case of $BaTiO_3$, to make it co-sinterable with nickel electrodes. In this system, the transition metal is easily reduced to form Ti^{3+}/Ti^{2+} ions, which induces oxygen vacancies and gives rise to poor insulating resistance. It is then necessary to compensate for this contribution by introducing acceptor dopants.[10–14] The same behavior is observed in other Ti based dielectrics such as $MgTiO_3$[15] and explains our choice of a zirconate, which is less sensitive to reduc-

* Corresponding author.
E-mail address: michael.pollet@ismra.fr (M. Pollet).

0955-2219/03/$ - see front matter © 2003 Elsevier Ltd. All rights reserved.
doi:10.1016/S0955-2219(03)00122-5

tion.[16,17] In order to lower the sintering temperature, several solutions have already been studied: the effect of the grain size of the raw materials,[18] the phase stoichiometry,[19,20] glass addition,[21] and doping.[22,23]

This study of $CaZrO_3$ can be divided in four parts: (i) the synthesis of the powder precursor of the perovskite phase; (ii) the sintering process at low temperature with the analysis of the grain size, stoichiometry, and addition of lithium salts; (iii) the effect of a reducing atmosphere on the dielectric material; and (iv) the Ni-cofired sample characterization.

2. Experimental procedures

The conditions used in the sample preparation, characterization and testing were as follows.

2.1. Precursors

Grade reagents (CERAC) $CaCO_3$ (99.95% purity) and ZrO_2 (99.95% purity) were chosen.

2.2. Mixing/milling

Powders were ball-milled in absolute ethanol using an agate mortar with agate balls for 3/4 h. The mixture was then dried under infrared lamps and de-agglomerated by hand in an agate mortar.

2.3. Shaping

The powders are granulated with an organic binder (polyalcohol) and uniaxially pre-densified to green discs. 6.36 mm dia. discs for dilatometric measurements were pressed under a charge of 2100 kg (≈648.5 MPa). 8.06 mm dia. discs for sintering were pressed under a charge of 3880 kg (≈746 MPa).

2.4. Dilatometric measurements and sintering

Dilatometric measurements were carried out in static air (SETARAM TMA92 dilatometer). For all the measurements, the temperature was raised and lowered at 2°/min with a dwell at 1500 °C for 1 h. A heat/cool ramp of 2.5°/min was chosen for the sintering in a tube furnace, with a thermal cycle (dwell temperature and duration) dependent upon the dilatometric results. The sintering atmosphere was air (static) or a moisture saturated at room temperature (RT) mixture composed of 10%H_2/90% Ar.

2.5. Thermogravimetric analysis (TGA)

TGA measurements were carried out using a SETARAM TGDTA92 analyzer.

2.6. Cofired sample preparation

Two 8.06 mm dia. discs were prepared (around 1 mm thickness). One face of each was painted with a mix of nickel nanometric powder and organic binder. The painted faces were placed in contact with each other and the two discs were pressed together under a charge of 3880 kg.

2.7. X-ray diffraction

All of the synthesized powders and discs were analyzed by X-ray diffraction either with a Guinier camera (ENRAF NONIUS FR590) or with a SEIFERT diffractometer (copper $K\alpha_1$ radiation).

2.8. Microstructure analysis

The samples were observed under a polarized optical microscope (Olympus BH2-HLSH). For scanning electron microscopy (SEM), the samples were polished and thermally etched at 1000 °C (ramp 1 h, dwell 30 min, cool to room temperature in 1 h). They were then gold-sputtered and observed with a Philips XL30 FEG SEM.

2.9. Grain size determination

The grain size of the powders was measured using a Mastersizer laser granulometer (MALVERN). It contains 64 uniformly spaced sizebands on a logarithmic plot in a range between 0.1 and 600 μm.

2.10. Composition analysis

Phase composition was obtained via energy dispersive spectroscopy (EDS) using a Jeol 200CX. Quantitative analysis was carried out by atomic absorption (VARIAN SpectrAA-20 spectrometer).

2.11. Electrical measurements

Shaped discs were painted on both faces with an In-Ga eutectic paste and dried in an oven at 120 °C. Insulating resistance measurements were obtained using a SEFELEC DM500A megohmmeter. The dielectric characteristics were acquired with a FLUCKE 6306 LCR meter. The temperature-dependence measurements also required a drying oven (SECASI).

2.12. Magnetic measurements

The magnetic susceptibility was measured using a SQUID magnetometer (Quantum Design MPMS 5) from 70 to 300 K.

3. Results and discussion

3.1. The powder precursor synthesis

When using ZrO_2 and $CaCO_3$ precursors, a calcination step is necessary to eliminate CO_2 before the sintering step in order to ensure a dense sample,[2] because the departure of CO_2 results in a porous pellet. The dependence of phase formation on calcination parameters was investigated. The milled precursor powders were placed in cylindrical alumina crucibles, and the effects of calcination temperature, dwell duration and heating rate were analyzed.

To evaluate temperature dependence, all the samples were heated simultaneously at a rate of 1°/min, then each sample was removed from the furnace at a specific temperature (700, 800, 900, 1000, 1040, 1100, 1140, 1200 and 1300 °C) and quenched to room temperature in air. The weight change was evaluated, and the powder was characterized by X-ray diffraction. The $CaCO_3/ZrO_2$ mixture's weight loss versus temperature behavior is typical of decomposition with gas departure and corresponds well to the results of thermogravimetric analysis (Fig. 1). Indeed, the losses are well matched to the temperature decomposition of $CaCO_3$ into CaO. Furthermore, the calculated theoretical weight loss ($=1-M(CaZrO_3)/([M(CaCO_3) + M(ZrO_2)]) = 19.7\%$), assuming the weight loss is solely due to the departure of CO_2, corresponds to the experimentally observed loss.

This similar evolution versus temperature of the mixture and of $CaCO_3$ alone (same curve shape) shows that $CaCO_3$ loses CO_2 before reacting with ZrO_2 (in which case evidence of the decomposition of a $(Ca,Zr)CO_z$ phase would be seen).

The X-ray diffraction patterns of the calcined samples can be found in Fig. 2. Table 1 lists the main peaks of the various phases present in the mixtures. The lowest X-ray pattern (Fig. 2) corresponds to the mixture at room temperature. At 800 °C, a new peak appears at 37.35°, corresponding to the [200] peak of CaO (indicated by the arrow). The growth of this peak is directly linked to the intensity decrease of the $CaCO_3$ [104] peak. as CaO forms, the ZrO_2 [-111] peak decreases in intensity and a new peak belonging to the $CaZrO_3$ phase appears (the [200] peak).[24] The CaO [200] peak is visible until 1040 °C, when it is replaced by the low intensity [130] and [211] peaks of $CaZrO_3$.

The higher temperature samples were also analyzed in order to confirm the formation of secondary phases. At 1040 °C, a line of very low intensity appears towards 30.2°. It may be attributed to a $Ca_xZr_yO_{2x+4y}$ phase ($x/y<1$; for instance $Ca_{0.15}Zr_{0.85}O_{1.85}$[25]), but given the lack of information (only one peak) no definitive conclusion can be given. Moreover, this peak disappears entirely at 1300 °C, and only the $CaZrO_3$ phase remains. These results agree with those obtained by TGA concerning both the decomposition of $CaCO_3$ to form CaO and the solid phase reaction between CaO and ZrO_2 to synthesize the $CaZrO_3$ phase.

Based on the above results, the dwell temperature was fixed at 1000 °C, since further heating only seems to increase the phase crystallinity. This temperature was

Table 1
Miller's indices and the corresponding 2θ for phases discussed in text

Phase	Peak	2θ
CaO	200	37.35°
$CaCO_3$	104	29.37°
ZrO_2	−111	28.22°
$CaZrO_3$	200	31.99°
	130	37.26°
	211	37.44°

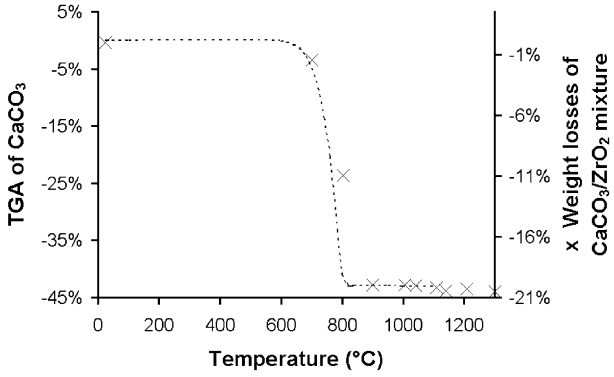

Fig. 1. Weight loss vs. temperature of $CaCO_3$–ZrO_2 mixture (x) and $CaCO_3$ TGA's curve (dotted curve).

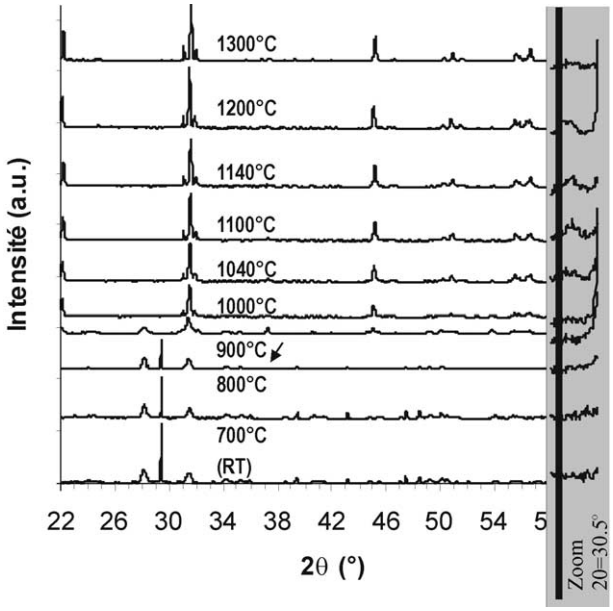

Fig. 2. X-ray diffraction patterns of $CaCO_3$–ZrO_2 mixture at various temperatures.

maintained for 0, 1, 2 and 3 h. The heating rate was still 1°/min. The samples were quenched in air and analyzed. In all cases, the weight loss accounts for the complete removal of CO_2 from $CaCO_3$. The X-ray patterns show that the $CaZrO_3$ phase forms after 2 h. A final test was carried out by heating at a rate of 150°/h to 1000 °C and calcining for 2 h. The resulting X-ray diffraction pattern shows little difference from that of the slower ramp, except for a small persistence of precursors.

As a result of these experiments, the heating profile chosen for the calcination of the $CaZrO_3$ precursor powder is: 150°/h to 1000 °C, 2 h dwell, 150°/h to RT.

3.2. Sintering process at low temperature

Precursor powder was prepared using the procedure described in the previous section. In order to minimize the grain size of the powder, powders were milled in an agate mortar for varying durations (Table 2). After milling, the grain size was measured before thermal treatments. Fig. 3 shows the grains Sauter Mean Diameter and Herdan Mean Diameter [Eq. (1)] versus milling duration. One can see that a duration longer than 45 min is not necessary since no evolution is observed after this point. The SEM micrograph (Fig. 4) shows that the grain size obtained is about 200 nm for durations $\geqslant$45 min.

$$\begin{aligned}&\text{Sauter Mean Diameter} = D[3,2]\\&\quad(= 6/\text{Specific Surface Area})\\&\\&\text{Herdan Mean Diameter} = D[4,3]\\&\quad(= \text{Mean Diameter over the Volume distribution})\end{aligned} \tag{1}$$

where $D[m,n] = \left[\frac{\sum V_i d_i^{m-3}}{\sum V_i d_i^{n-3}}\right]^{\frac{1}{m-n}}$ and V_i is the volume and d_i the mean diameter of a sizeband i.

Our dilatometric measurements show, unsurprisingly, that the smaller the grain size, the sooner the pellet shrinkage commences (Fig. 5). Decreasing the grain radius could perhaps lower the sintering temperature below the melting point of nickel (1453 °C), unfortunately, milling is not sufficient to achieve this goal, but chemical preparation methods can be used to obtain smaller particles.[26]

The shrinkage behavior described above pertains to all of the samples measured, except G45 (not plotted since its behavior is nearly the same as G90) and G90.This behavior may be due to the aging of the powder since these samples, prepared at the same time as the others and with no particular conservation procedure, were the last to be studied with the dilatometer. A new dilatometric measurement made on the G120 sample, 1 month after the first one, confirms this idea

Table 2
$CaCO_3/ZrO_2$ mixture milling duration

Sample	Milling duration (min)	Comments
G0	0	Large particles (≈1 μm)
G5	5	Fine + large particles
G15	15	Fine + large particles
G30	30	Fine + large particles
G45	45	Fine particles
G60	60	Fine particles
G90	90	Fine particles
G120	120	Fine particles (≈200 nm)

The sample name for each milling duration is "G" for "grain" followed by a number corresponding to the milling duration in minutes.

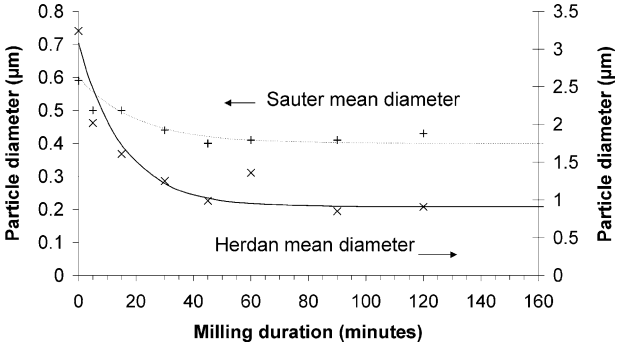

Fig. 3. Sauter (+) and Herdan (x) mean diameter after milling versus milling duration of undoped stoichiometric $CaZrO_3$.

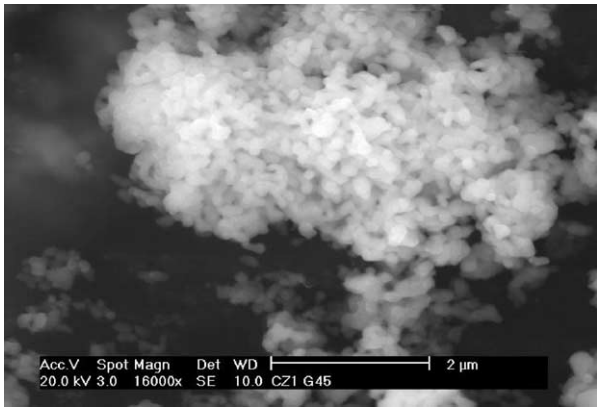

Fig. 4. $CaZrO_3$ calcined powder after 45 min milling.

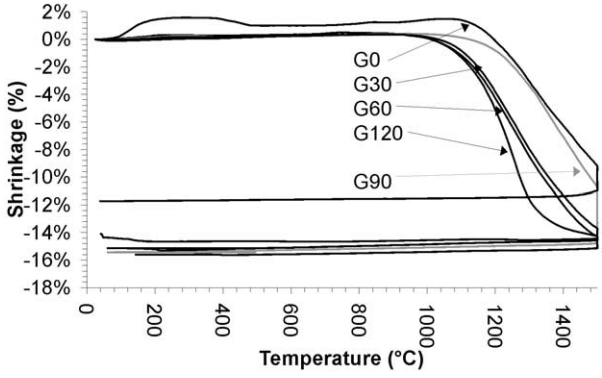

Fig. 5. Shrinkage curves for various milling durations.

with a dilatometric curve shifted to higher temperature. Further investigations should be made to clarify this point.

Based on both dilatometric results and the need for a lower sintering temperature, all these samples were sintered in static air at 1400 °C for 6 h. Densities, geometrically measured, are about 95% of the theoretical density. However, SEM micrographs show that with increasing milling duration, porosity slightly decreases. Moreover, whereas the grain size is about 2 μm for the non-milled sample (G0), this size reaches less than 1 μm for samples milled for at least 45 min (Fig. 6). Since this material is to be used in MLCCs, in which dielectric layers can not exceed 20 μm in thickness, it is important to reduce the grain size in such a way as to increase the number of grain boundaries (between metallic layers) which act as electrical barriers.

The samples which have been thermally etched display crystallites on their surfaces (Fig. 6), for which the cationic composition determined with EDS is Ca/Zr = 55/45. The phase of these crystals has not been identified. However, it has been shown that these crystals were only present on thermally etched samples.

The electrical and dielectric measurements made on the sintered samples are encouraging. The insulating resistivity is between 5×10^{13} and 11×10^{13} Ω.cm. The dielectric constant (K) is about 28.5 and losses are less than 0.2% at 1 kHz (at 1 MHz, $K\approx29$ and losses are less than 0.1%). As a result of the above experiments, the samples discussed below were all milled for 45 min before sintering. Although this duration may not be the optimum, it is the point corresponding to the reaching of the asymptotic behavior in the granulometric measurements. This duration results in both fine particles in powder precursor and fine grains in the sintered material.

Another parameter investigated to lower the sintering temperature of $CaZrO_3$ was the stoichiometry. Non-stoichiometry was introduced either before sintering, i.e. a mixture of $CaCO_3+(1-x)ZrO_2$ was calcined, or it was introduced after calcination by the addition of $CaCO_3$ or ZrO_2 to the pure calcined phase. For the first case, a mixture of $CaCO_3+(1-x)ZrO_2$, where x can be positive or negative (Table 3), was milled and calcined using the parameters described in the first section (±150°/h; 2 h at 1000 °C). After calcination, the powders were analyzed by X-ray diffraction and then milled again for 45 min. In all cases, $CaZrO_3$ is obtained with a small amount of residual precursor (ZrO_2 and CaO). The stoichiometry has a slightly effect on the X-ray patterns (difference in the threshold).

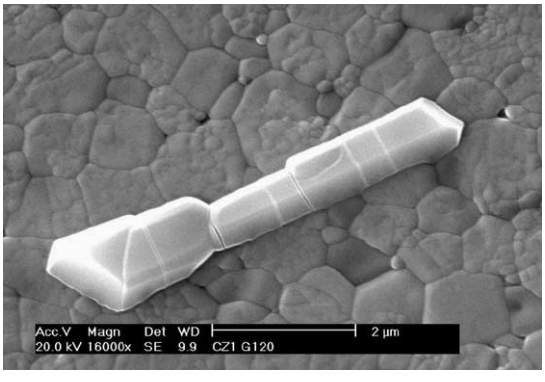

Fig. 6. SEM photograph of sample G120 after sintering.

The calcined powders were then studied using the dilatometer. derivative curves were calculated in order to compare the behavior of the pellets. The comparison point chosen was the temperature required to achieve the maximum shrinkage rate. It appears that the non-stoichiometry has the expected influence on the shrinkage behavior (Fig. 7a). In fact, all curves representative of a deficient composition are shifted to lower temperature with differences at least of 80 K. For the calcium-deficiencies, the shift reaches a maximum of 100 K for almost all tested compositions. On the contrary, for the zirconium-deficient materials, the shift evolves with the composition: for the smallest deficiencies (<2%), the shift is maximum (150 K) and decreases when the calcium amount increases. This behavior could be interpreted in terms of facilitated diffusion through the defected lattice, where ion mobility is perhaps increased. This interpretation does not explain the difference between the smallest and the highest zirconium-deficiencies. Nevertheless, this interpretation is supported by the dielectric measurement results on 1400 °C sintered samples. They show a slight increase in the loss (0.7–0.8% versus 0.4% for the stoichiometric phase at 1 kHz) in the same field of deficiency. This increase is correlated with anharmonic lattice vibrations, which develop in the presence of excess vacancies.[27] These results, not confirmed by XRD, suggest the existence of a sharp domain of solid solution centered at around the 1% zirconium-deficient composition. The permittivity is

Table 3
Compositions of samples $CaCO_3+(1-x)ZrO_2$ for which the non-stoichiometry was introduced before calcination

Sample	x (%)	Comment
CZ-10	−10	Ca deficiency with a theoretical composition as $Ca_{[1/(1-x)]}ZrO_{[(3-2x)/(1-x)]}$
CZ-5	−5	
CZ-1	−1	
CZ0	0	Stœchiometric phase
CZ02	0.2	Zr deficiency with a theoretical composition as $CaZr_{1-x}O_{3-2x}$
CZ05	0.5	
CZ06	0.6	
CZ1	1	
CZ2	2	
CZ5	5	
CZ10	10	
CZ50	50	

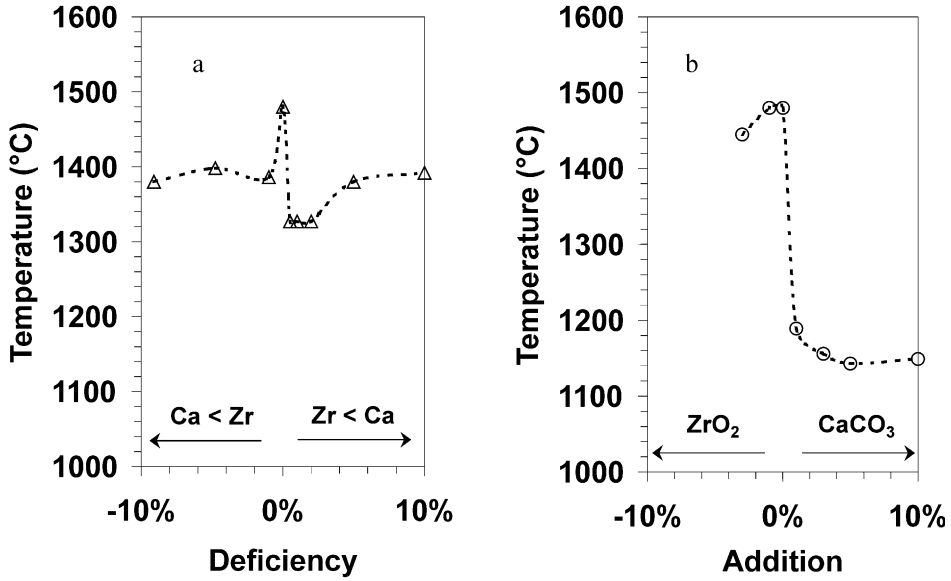

Fig. 7. (a) Maximum shrinkage rate temperature for the samples for which non-stoichiometry is affected before calcination. (b) Maximum shrinkage rate temperature for the samples in which non-stoichiometry was induced post-calcination.

constant regardless of the stoichiometry (≈30), except in the sample with a high deficiency value (CZ50; Table 3) where it decreases (≈25).

Experiments were also performed to observe the effects of a small amount of precursor addition (either $CaCO_3$ or ZrO_2) on the $CaZrO_3$ stoichiometric phase (Table 4). Again, the maximum shrinkage rate temperatures, measured on derivative curves, were chosen as comparison points. These points are plotted versus the precursor addition in Fig. 7b. By convention, and to simplify the comparison with the previous case, the plot's abscissa is negative for ZrO_2 addition and positive for $CaCO_3$ addition. ZrO_2 addition results in a slight shift of up to 35 K for the highest doped sample (3 mol%). But the most interesting result is due to $CaCO_3$ addition, which affects a shift as high as 300 K for a doping rate of 5 mol%. Moreover this shift is accompanied by an increase of the shrinkage rate that reaches a value 7 times higher than the one obtained with the undoped phase. The shrinkage curves, $\Delta L/L_0$ versus temperature, also show that $CaCO_3$ addition to the $CaZrO_3$ phase lowers the sintering temperature to approximately 1300 °C. Dielectric measurements are similar to those obtained from the stoichiometric phase.

A final means explored to reduce the sintering temperature was the addition of lithium salts.[25] The salts used were LiF, Li_2CO_3 or $LiNO_3$. These sintering agents were added at a concentration of 5 mol% to the $CaZrO_3$ powder, milled for 45 min and then shaped into discs. The density evolution and the relative densification rate curves are reported in Fig. 8. In all cases, the temperature at which the maximum rate of shrinkage occurs is substantially below that of the undoped material. Li_2CO_3 or $LiNO_3$ compositions seem to exhibit similar densification behavior, with the densification process ending near 1250 °C. On the other hand, the LiF-doped composition behaves differently: first, it shrinks quickly until the temperature reaches 1270 °C, then the sample shrinks more gradually until the end of the thermal cycle. The weight losses of each sample are nearly equal to the weight of the added dopant, which implies that

Table 4
Precursor addition quantities to stoichiometric $CaZrO_3$ phase

Sample	%mol	Comment
Z3	3	ZrO_2 addition
Z1	1	
CZ0	0	No addition
C1	1	$CaCO_3$ addition
C3	3	
C5	5	
C10	10	

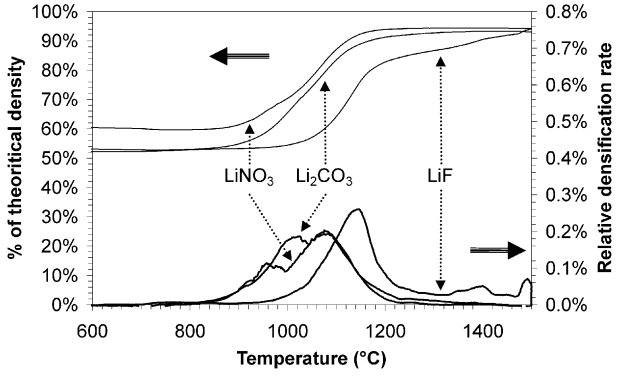

Fig. 8. Density evolution and relative densification rate curves versus temperature for compositions containing lithium salts.

the Li salt is eliminated during the sintering process. Atomic absorption measurements of the LiF-doped sample verify that the amount of remaining lithium is less than the detection threshold.

The samples were sintered at 1200 °C for 12 h. The relative densities reached at the end of this treatment are ~96% for the $LiNO_3$-doped sample, 93% for the Li_2CO_3 one and ~81% for the LiF one. The electrical measurements follow the same trend as the densities, the best material being the $LiNO_3$-doped sample, which achieves dielectric parameters nearly equal to those of the CaZrO3 phase ($\varepsilon \sim 32$, $tg\delta < 0.1\%$, $\alpha_T \sim 0$ ppm/K at 1 MHz). However, the microstructures reveal that this last sample has been heated at too high temperature (or for a too long time) since the grain size reaches 2 μm (versus 1 μm for the not completely sintered LiF-doped sample) (Fig. 9) and since large coalesced pores are visible. These observations imply that the temperature (or dwell duration) should be decreased which could be detrimental to a good density.

3.3. The effect of a reducing atmosphere on the $CaZrO_3$ material

The effect of the reducing atmosphere was studied using thermogravimetric analysis (TGA)[28] and magnetic susceptibility analysis.[29,30] $CaZrO_3$ powder was calcined and annealed at 1000 °C either in static air or reducing atmosphere [10%H_2/90% Ar; moisture saturated]. The resulting powder was then analyzed with TGA using the opposite atmosphere (i.e. O_2 if annealed in reducing atmosphere and Ar/H_2 moisture saturated at RT if annealed in static air). If the sample annealed in the reducing atmosphere was indeed reduced, the TGA treatment in air should re-oxidize the material, which should result in a weight gain due to oxygen introduction in the structure. On the contrary, there should be a minimum number of oxygen vacancies in the structure annealed in air so that the treatment in the reducing atmosphere should create an oxygen departure, and a weight loss will be observed. The results are displayed in Fig. 10. They show that the behavior is independent of the annealing atmosphere. There is a slight weight loss (less than 0.2%, or 1 mg, for the samples used) in both cases that may be attributed to H_2O departure. Thus, no atmosphere-dependant is observed in the case of $CaZrO_3$.

The magnetic susceptibility was also studied on $CaZrO_3$ calcined powders, both untreated and annealed at 1000 °C in a reducing atmosphere [10%H_2/90% Ar; moisture saturated]. $1/\chi$ versus T is plotted in Fig. 11. This analysis reveals no differences in susceptibility between the two powders. Moreover, a simple calculation shows that the magnetic susceptibility measured in the constant field (150–300 K) is equal to the sum of the individual diamagnetic contributions of all the ions (data from Ref. 31):

$$\chi_{\text{Constant}} = 52.10^{-6} \text{ emu/mole/Gauss} \chi_{\text{CaZrO3}} = \sum \chi_i$$

$$= \chi_{Ca^{2+}} + \chi_{Zr^{4+}} + 3.\chi_{O^{2-}}$$

$$\chi_{\text{CaZrO3}} = (8 + 10 + 3.12).10^{-6}$$

$$= 54.10^{-6} \text{ emu/mole/Gauss}$$

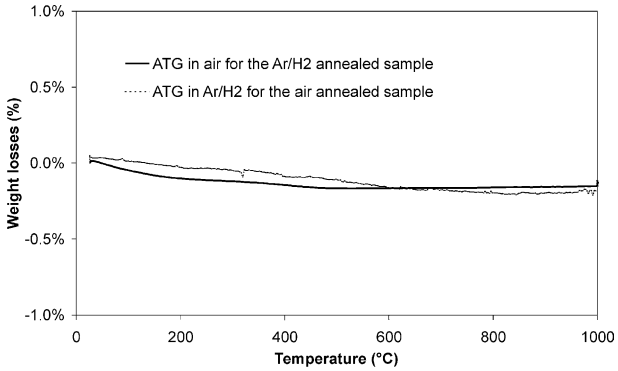

Fig. 10. TGA results for $CaZrO_3$ versus atmosphere used during heating treatment.

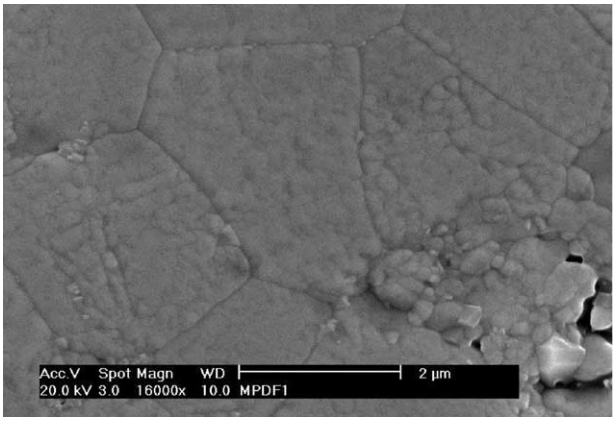

Fig. 9. Microstructure of the 5 mol% $LiNO_3$-doped sample.

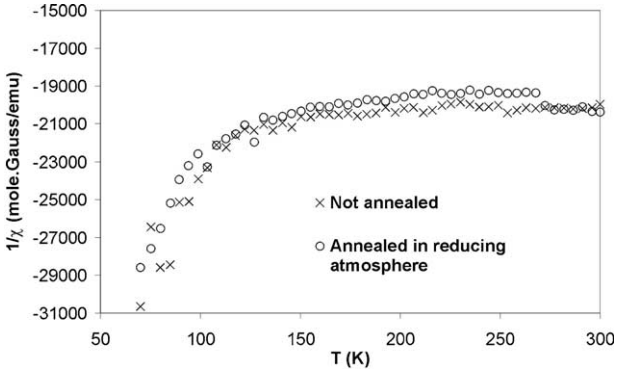

Fig. 11. Inverse of magnetic susceptibility versus temperature as a function of the atmosphere used during heating treatment of $CaZrO_3$ calcined powders.

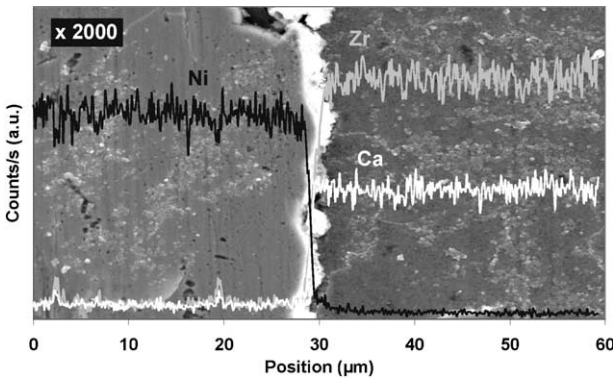

Fig. 12. SEM observation and EDS analysis of the Ni-($CaZrO_3$ + 5%mol.$CaCO_3$) co-sintered material.

If the hypothetical contribution of reduced Zr^{4+} to Zr^{2+} is taken into account, it would only increase the susceptibility since $\chi_{Zr^{2+}} = 47.4 \times 10^{-6}$ emu/mole/Gauss[31] so this hypothesis can be rejected.

Considering both TGA and magnetic susceptibility results, the resistance to reduction of $CaZrO_3$ is confirmed. Moreover, dielectric and electrical measurements on samples sintered in both static air and the reducing atmosphere display no differences between the samples. The good properties of $CaZrO_3$, regardless of the sintering atmosphere simplify its use as a base-metal co-sinterable material, since there is no need to search for a compensating doping agent as is the case with titanates.

3.4. The Ni-cofired sample characterization

Based on results above, a Ni-cofired sample was prepared. The dielectric composition is a mixture of the $CaZrO_3$ stoichiometric phase and an addition of 5 mol% $CaCO_3$. The co-sintered material was heated to 1300 °C for 2 h at a rate of 150 K/h. The SEM/EDS results are summarized in Fig. 12. The line-scan carried out with the EDS shows that the interface between the dielectric and the metal is abrupt and that no matter has diffused between these two materials, with respect to the analyzer sensitivity (1 μm). This is an important result since it proves the manufacturability of Ni-co-sintered MLCC.

4. Conclusion

The $CaZrO_3$ phase synthesis has been optimized with the cycle [150 K/h, 1000 °C for 2 h, −150 K/h to RT]. The phase obtained is almost pure with a slight remainder of precursors. The standard aids to sintering have been tested. The grain size reduction using a wet-ball-milling has been optimized in order to increase the reactivity, and it was confirmed that a small grain powder (close to 200 nm) could lower the sintering temperature even though the required temperature reached is still too high. The effect of the stoichiometry was investigated and revealed the presence of a solid solution in a small domain centered near the 1% zirconium-deficient composition. The sintering temperature is decreased in the field of this solid solution.

The effect of a small addition of precursors to the calcined stoichiometric composition has also been investigated. This study revealed that both ZrO_2 and $CaCO_3$ additions lower the sintering temperature, although the best result was obtained with the addition of $CaCO_3$, which brings the sintering temperature below 1300 °C. The effect of lithium salts was also considered. $LiNO_3$ was the best candidate to improve the sintering conditions with a sintering ending temperature of about 1250 °C.

The effect of the sintering atmosphere was investigated. Neither TGA, magnetic susceptibility, nor electric/dielectric measurements display any evidence of reduction of the zirconium from Zr^{4+} to Zr^{2+}, which precludes the need to add a compensating dopant, as it is the case for titanate-based materials. Finally, a Ni-co-sintered material was synthesized with the $CaZrO_3$ phase and a small addition of $CaCO_3$. EDS measurements have revealed no matter diffusion between the dielectric, leading to no degradation of the dielectric properties of the material.

Acknowledgements

The authors wish to thank the TEMEX Society for supporting this work.

References

1. Suzuki, Y., Morgan, P. E. D. and Ohji, T., New uniformly porous CaZrO3/MgO composites with three-dimensional network structure from natural dolomite. *Journal of the American Ceramic Society*, 2000, **83**(8), 2091–2093.
2. De Pretis, A., Ricciardiello, F. and Sbaizero, O., Mechanical properties of polycrystalline CaZrO3. *Powder Metallurgy International*, 1986, **18**(6), 427–430.
3. Lim, Sang-Kyu, Lee, Han-Young, Kim, Jun-Chul and An, Chul, The design of a temperature-stable stepped-impedance resonator using composite ceramic materials. *IEEE Microwave and Guided Wave Letters*, 1999, **9**(4/April), 143–144.
4. Yamagushi, T., Komatsu, Y., Otobe, T. and Murakami, Y., Newly developed ternary (Ca,Sr,Ba) zirconate ceramic system for microwave resonators. *Ferroelectrics*, 1980, **27**, 273–276.
5. Borglum, B. P. and Buchanan, R. C., SEM determination of optimum processing conditions for microwave dielectrics in the (Ca,Sr,Ba) zirconate system. In *Proceedings of the 45th Annual Meeting of the Electron Microscopy Society of America*, ed. G.W. Bailey. San Francisco Press, 1987, pp. 372–373.
6. Wang, C., Xu, X., Yu, H., Wen, Y. and Zhao, K., A study of the solid electrolyte Y2O3-Doped CaZrO3. *Solid State Ionics*, 1988, **28–30**, 542–545.
7. Engelen, W., Buekenhoudt, A., Luyten, J. and De Shutter, F.,

Humidity sensitivity of electrochemical hydrogen cells using calcium zirconate ceramics. *Solid State Ionics*, 1997, **96**, 55–59.
8. Kobayashi, Kiyoshi, Yamaguchi, Shu and Iguchi, Yoshiaki, Electrical transport properties of calcium zirconate at high temperature. *Solid State Ionics*, 1998, **108**, 355–362.
9. Higuchi, T., Tsukamoto, T., Tezuka, Y., Kobayashi, K., Yamagushi, S. and Shin, S., Photoemission study of the exchange mechanism of proton and hole. *Japonese Journal of Applied Physics*, 2000, **39**, L133–L136.
10. Albertsen, K., Hennings, D. and Steiglemann, O., Donor-acceptor charge complex formation in barium titanate ceramics: role of firing atmosphere. *Journal of Electroceramics*, 1998, **2**(3), 193–198.
11. Hansen, P., Hennings, D. and Schreinemacher, H., Dielectric properties of acceptor-doped (Ba,Ca)(Ti,Zr)O3 ceramics. *Journal of Electroceramics*, 1998, **2**(2), 85–94.
12. Hansen, P., Hennings, D. and Schreinemacher, H., High-K dielectric ceramics from donor/acceptor-codoped (Ba1-xCax)(Ti1-yZry)O3 (BCTZ). *Journal of the American Ceramic Society*, 1998, **81**(5), 1369–1373.
13. Lee, W. H., Tseng, T. Y. and Hennings, D., Effects of calcination temperature and A/B ratio on the dielectric properties of (Ba,Ca)(Ti,Zr,Mn)O3 for multilayer ceramic capacitors with nickel electrodes. *Journal of the American Ceramic Society*, 2000, **83**(6), 1402–1406.
14. Lee, Wen-Hsi, Tseng, Tseung-Yuen and Hennings, D., Effects of A/B cation ratio on the Microstructure and Lifetime of (Ba1-xCax)z(Ti0,99-yZryMn0,01)O3 (BCTZM) sintered in reducing atmosphere. *Journal of Materials Science: Materials in Electronics*, 2000, **11**, 157–162.
15. Vigreux, C., Deneuve, B., El Fallah, J. and Haussonne, J. M., Effects of acceptor and donor additives on the properties of MgTiO3 ceramics sintered under reducing atmosphere. *Journal of the European Ceramic Society*, 2001, **21**(10–11), 1681–1684.
16. Davies, R. A., Islam, M. S. and Gale, J. D., Dopant and proton incorporation in perovskite-type zirconates. *Solid State Ionics*, 1999, **126**, 323.
17. Nadler, M. R. and Fitzsimmons, E. S., Preparation and properties of calcium zirconate. *Journal of the American Ceramic Society*, 1995, **38**(6), 214–217.
18. Yan, M. F., Microstrutural control in the processing of electronic ceramics. *Materials Science and Engineering*, 1981, **48**, 53–72.
19. Lee, W. H., Tseng, T. Y. and Hennings, D., Effects of calcination temperature and A/B ratio on the dielectric properties of (Ba,Ca)(Ti,Zr,Mn)O3 for multilayer ceramic capacitors with nickel electrodes. *Journal of the American Ceramic Society*, 2000, **83**(6), 1402–1406.
20. Lee, Wen-Hsi, Tseng, Tseung-Yuen and Hennings, D., Effects of A/B cation ratio on the microstructure and lifetime of (Ba1-xCax)z(Ti0,99-yZryMn0,01)O3 (BCTZM) sintered in reducing atmosphere. *Journal of Materials Science: Materials in Electronics*, 2000, **11**, 157–162.
21. Kanai, H., Furukawa, O., Nakamura, S. I. and Yamashita, Y., Effects of B2O3 and SiO2 on dielectric properties and reliability of a lead-based relaxor dielectric ceramic. *Journal of Materials Science*, 1996, **31**, 1609–1614.
22. Haussonne, J. M., Regreny, O., Lostec, J., Desgardin, G., Halmi, M., Raveau, B., Sintering of various perovskites with lithium salts. In *6th CIMTEC, World Congress on Hightech Ceramics*, June, 1986.
23. Haussonne, J. M. and Desgardin, G., Dielectric properties of barium titanate-based capacitors with lithium additions. *Dielectric Ceramics*, 1992, 155–165.
24. Koopmans, J. A., Van De Velde, G. M. H. and Gellings, P. J., Powder neutron diffraction study of the perovskites CaTiO3 and CaZrO3. *Acta Crystallographica C*, 1983, **39**, 1323–1325.
25. Joseph, M., Sivakumar, N., Manoravi, P. and Vanavaramban, S., Preparation of thin film of CaZrO3 by pulsed laser deposition. *Solid State Ionics*, 2001, **144**, 339–346.
26. Le, J., van Rij, L. N., van Landschoot, R. C. and Schoonman, J., A wet-chemical method for the synthesis of In-doped CaZrO3 ceramic powder. *Journal of the European Ceramic Society*, 1999, **19**, 2589–2591.
27. Wakino, K., Sagala, D. A. and Tamura, H., Far infrared reflection spectra of Ba(ZnTa)O3 dielectric resonator material. *Japonese Journal of Applied Physics*, 1985, **24**, 1042–1044.
28. Hagemann, H. J. and Hennings, D., Reversible weight change of acceptor-doped BaTiO3. *Journal of the American Ceramic Society*, 1981, **64**(10), 590–594.
29. Ihrig, H., The phase stability of BaTiO3 as a function of doped 3d elements: an experimental study. *Journal of Physics: Condensed Matter*, 1978, **11**, 819–827.
30. Hagemann, H. J. and Ihrig, H., Valence change and phase stability of 3d-doped BaTiO3 annealed in oxygen and hydrogen. *Physical Review B*, 1979, **20**(9), 3871–3878.
31. Selwood, P. W., *Magnetochemistry*, 2nd edn. Interscience Publishers, New York, London, 1956.